Article

The Effect of the Particle Size on the Kinetics of CO Electrooxidation on High Surface Area Pt Catalysts

Matthias Arenz, Karl J. J. Mayrhofer, Vojislav Stamenkovic, Berislav B. Blizanac, Tada Tomoyuki, Phil N. Ross, and Nenad M. Markovic

J. Am. Chem. Soc., **2005**, 127 (18), 6819-6829• DOI: 10.1021/ja043602h • Publication Date (Web): 16 April 2005

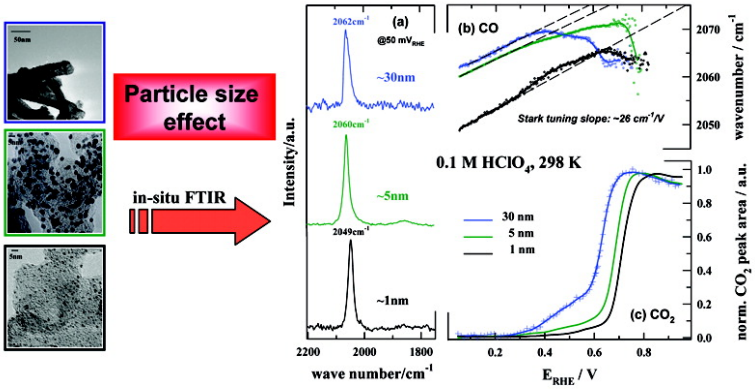

More About This Article

Additional resources and features associated with this article are available within the HTML version:

- Supporting Information
- Links to the 14 articles that cite this article, as of the time of this article download
- Access to high resolution figures
- Links to articles and content related to this article
- Copyright permission to reproduce figures and/or text from this article

View the Full Text HTML

J|A|C|S
ARTICLES
Published on Web 04/16/2005

The Effect of the Particle Size on the Kinetics of CO Electrooxidation on High Surface Area Pt Catalysts

Matthias Arenz,*,†,§ Karl J. J. Mayrhofer,† Vojislav Stamenkovic,† Berislav B. Blizanac,† Tada Tomoyuki,‡ Phil N. Ross,† and Nenad M. Markovic†

Contribution from the Materials Science Division, Lawrence Berkeley National Laboratory, University of California, Berkeley, California 94720, and Tanaka Kikinzoku Kogyo K. K. Cooperation (TKK), Tokyo, Japan

Received October 21, 2004; E-mail: matthias.arenz@ch.tum.de

Abstract: Using high-resolution transmission electron microscopy (TEM), infrared reflection−absorption spectroscopy (IRAS), and electrochemical (EC) measurements, platinum nanoparticles ranging in size from 1 to 30 nm are characterized and their catalytic activity for CO electrooxidation is evaluated. TEM analysis reveals that Pt crystallites are *not* perfect cubooctahedrons, and that large particles have "rougher" surfaces than small particles, which have some fairly smooth (111) facets. The importance of "defect" sites for the catalytic properties of nanoparticles is probed in IRAS experiments by monitoring how the vibrational frequencies of atop CO (ν_{CO}) as well as the concomitant development of dissolved CO_2 are affected by the number of defects on the Pt nanoparticles. It is found that defects play a significant role in CO "clustering" on nanoparticles, causing CO to decrease/increase in local coverage, which yields to anomalous redshift/blueshift ν_{CO} frequency deviations from the normal Stark-tuning behavior. The observed deviations are accompanied by CO_2 production, which increases by increasing the number of defects on the nanoparticles, that is, $1 \leq 2 < 5 \ll 30$ nm. We suggest that the catalytic activity for CO adlayer oxidation is predominantly influenced by the ability of the surface to dissociate water and to form OH_{ad} on defect sites rather than by CO energetics. These results are complemented by chronoamperometric and rotating disk electrode (RDE) data. In contrast to CO stripping experiments, we found that in the backsweep of CO bulk oxidation, the activity increases with decreasing particle size, that is, with increasing oxophilicity of the particles.

1. Introduction

The size-dependent catalytic properties of metal nanoparticles play a vital role in emerging technologies for environmental and energy related applications, such as fuel cells. The characteristic dimension of metal clusters employed in fuel cells is in the size range of a few nanometers. Because the electronic properties of metal aggregates in this size range do not differ from those of the bulk metal,[1,2] catalyst research of such materials has focused on the variation of the surface structure of metal aggregates with their size, that is, how the proportions of different types of adsorption sites (facets) vary with dimension for a given structure. There is no simple ideal structure that will necessarily model all the aspects of nanoparticle catalysts, particularly in the exact configuration as they are used in electrolytic cells. However, if the equilibrium shape of a nanoparticle, as is the case for the fcc metal Pt, is a cubo-octahedral structure consisting of (111) and (100) facets bound by edge atom rows that are like the topmost rows of the (110) surface, then well-characterized single-crystal surfaces may be used as reasonable models.[3] Many research groups have used this strategy to predict what the particle size might be, that is, the variation of the reaction rate or selectivity with the characteristic dimension of metallic clusters at the electrified solid−liquid interface. For example, given the well-documented sensitivity of the vibrational properties of adsorbed CO to its chemical and electrostatic environment, infrared reflection−absorption spectroscopy (IRAS) of CO adsorbed on ordered Pt single crystals has been used to understand how the properties of Pt nanoparticles depend on their size.[4−6] Further insight into the particle size effect has been obtained by electrochemical-based experiments, for example, monitoring CO adlayer oxidation, dubbed "CO stripping", on Pt nanoparticles in the size range of 1−10 nm.[7−10]

† University of California, Berkeley.
‡ TKK.
§ Present address: Chair Physical Chemistry I, Chemsitry Department, Technical University, Munich, Germany.

(1) Henry, C. R. *Surf. Sci. Rep.* **1998**, *31*, 231−325.
(2) Somorjai, G. A. *Introduction to Surface Chemistry and Catalysis*; John Wiley & Sons: New York, 1993.
(3) Markovic, N. M.; Ross, J. *Surf. Sci. Rep.* **2002**, *45*, 117−229.
(4) Chang, S. C.; Roth, J. D.; Ho, Y.; Weaver, M. J. *J. Electron Spectrosc. Relat. Phenom.* **1990**, *54*−*55*, 1185−1203.
(5) Lebedeva, N. P.; Rodes, A.; Feliu, J. M.; Koper, M. T. M.; van Santen, R. A. *J. Phys. Chem. B* **2002**, *106*, 9863−9872.
(6) Markovic, N. M.; Ross, P. N. *Electrochim. Acta* **2000**, *45*, 4101−4115.
(7) Friedrich, K. A.; Henglein, F.; Stimming, U.; Unkauf, W. *Colloids Surf., A* **1998**, *134*, 193−206.
(8) Cherstiouk, O. V.; Simonov, P. A.; Savinova, E. R. *Electrochim. Acta* **2003**, *48*, 3851−3860.
(9) Maillard, F.; Savinova, E. R.; Simonov, P. A.; Zaikovskii, V. I.; Stimming, U. *J. Phys. Chem. B* **2004**, *108*, 17893−17904.
(10) Maillard, F.; Eikerling, M.; Cherstiouk, O. V.; Schreier, S.; Savinova, E. R.; Stimming, U. *Faraday Discuss.* **2004**, 357−377.

Although this approach did provide some new insight into the structure sensitivity of CO oxidation,[7,9−16] in many cases, this tactic has also showed significant weaknesses. Probably the most notable example that the catalytic activities observed on single crystal surfaces cannot be used as specific one-to-one models for *real* nanoparticles has been CO monolayer oxidation (CO stripping) on Pt nanoparticles in acid electrolytes. In particular, it has been found that, although more oxophilic, smaller particles are less active than larger particles.[10] It was proposed that the reason for this observation is a stronger bonding of CO to the surface of smaller particles and a concomitant decrease in CO diffusion.[7,9,10,14,15]

An interesting yet largely unexplored issue in structure sensitivity is the importance of "defect" sites, which are inherently present on Pt single crystals[3,17] as well as on Pt nanoparticles.[18] For the onset of CO oxidation on Pt(*hkl*) (which is observed in the so-called "pre-ignition" potential region), we suggested that the kinetics are, in fact, determined predominately by the availability of defect sites on which adsorption of oxygenated species (hereafter denoted as OH) may occur.[3,17] Two other pieces of evidence point to the importance of defects in the surface chemistry of CO on Pt(*hkl*). The first is that domains of the observed surface structures of CO on Pt(111) are controlled by surface defects, that is, on less defected surfaces, larger domains of the p(2 × 2)−3CO structure[11] are observed. The second is that the potential-dependent vibrational behavior of CO (Stark-tuning) can be controlled by the number of surface defects, that is, a less defected surface exhibits an "anomalous" Stark-tuning slope.[19] The importance of defects in electrochemical reactions on Pt nanoparticles, however, has rarely been discussed. One exception is the work by Sattler and Ross[18] who showed that Pt crystallites are not perfect cubo-octahedrons and that real particles have rough surfaces, which provide a variety of different sites for catalysis.

Given the structural as well as spectral richness of the Pt−CO system, the examination of the effect of defects on Pt nanoparticles on the CO surface chemistry is of interest. Such a study of Pt nanoparticles in the size range of 1−30 nm is reported here. We demonstrate how the particle size-dependent number of defects in cubooctahedral particles affects the vibrational properties of CO and the CO_2 production during CO oxidation. We also consider how the electrocatalytic activity for CO oxidation changes with the experimental condition, such as an excess of OH_{ad} or CO on the catalyst surface.

2. Experimental Section

Catalyst Samples. Four different Pt high surface area catalysts were used in this study. Three samples, supplied by TKK (Tokyo, Japan), were carbon-supported Pt nanoparticles with mean diameters of 1−1.5, 2−3, and 5 nm, respectively (analysis by TKK). The fourth sample, consisting of a nanostructured Pt film supported on crystalline organic whiskers,[20] was supplied by 3M Company (St. Paul, MN U.S.A.). The particle size of the latter sample was roughly estimated to be about 30 nm based on the charge required to form a full monolayer of adsorbed hydrogen (the so-called H_{upd} charge). In the following, the catalysts will simply be denoted as 1, 2, 5, and 30 nm catalysts.

Electrochemical Measurements. The catalyst preparation has been described previously.[21] In short, the catalyst was dispersed ultrasonically in ultrapure water, and 20 μL of the suspension was pipetted onto a glassy carbon substrate (0.283 cm^2 geometrical surface area) leading to a Pt loading of 14 $\mu g_{Pt}/cm^2$ for the carbon-supported catalysts (TKK 1, 2, and 5 nm) and 42 $\mu g_{Pt}/cm^2$ for the 3M (30 nm) sample. The dried (Ar atmosphere) catalyst film was attached to the substrate by a thin Nafion film. The thus prepared surface was then transferred to the electrochemical cell protected by a drop of ultrapure water, immersed under potential control at 0.05 V in argon-saturated solution, and a cyclic voltammogram was recorded.

Two different procedures were used to form and oxidize a saturated CO adlayer on the Pt nanoparticles. In the first procedure, denoted hereafter as "oxide-annealing" (method I), before CO is adsorbed at 0.05 V, the catalyst was cycled in Ar-saturated solution (Air Products 5N5 purity) until a well-established cyclic voltammogram was observed. After forming a saturated CO adlayer (holding at 0.05V for 10 min in CO-saturated solution), the electrolyte was again purged with Ar (30 min), that is, the CO stripping curves are recorded in CO-free solution. In the second procedure, denoted hereafter as "CO-annealing" (method II), before adsorbing CO at 0.05 V and replacing CO by Ar, the electrode was "annealed" in CO-saturated solution by cycling of the electrode potential between $0.05 < E < 1.2$ V for 5 min. We used this experimental approach because we recently found that the CO-annealing pretreatment of Pt(111) may facilitate the removal of surface irregularities, which after the flame annealing preparation method are inherently present on the Pt(111) surface. As a consequence, upon CO-annealing of the (111) surface, the domain size of the p(2 × 2)−3CO structure, which is formed on Pt(111) at low potentials, is significantly improved.[3] As we demonstrate below, the catalytic and spectroscopic properties of high surface area catalysts pretreated by these two methods are completely different. Note, however, that the pretreatment is reversible, that is, the particles do not agglomerate during CO annealing. The stripping curves were recorded with a scan rate of 1 mV/s, and the upper potential limit was set to 1.0 V to guarantee the complete oxidation of the CO adlayer. Before the potentiodynamic measurements for the electrooxidation of CO gas dissolved in the electrolyte (CO bulk) were performed, the electrolyte was saturated by CO (1 atm) for 25 min while the electrode potential was held at 0.05 V. In chronoamperometric measurements, the electrooxidation rate of a saturated CO adlayer was measured in CO-free solution at a constant potential in order to further investigate the phenomena observed in stripping voltammetry. For each experiment, CO was adsorbed at 50 mV for 10 min under 1600 rpm, and then the CO current transients were recorded in Ar-saturated (15 min) solutions. The oxidation potential was chosen to be either in the preoxidation potential region, where depending on the electrode potential, the CO adlayer was completely or partially oxidized (see Supporting Information), or at/above the ignition potential, where CO was oxidized completely. Subsequently, CO stripping voltammetry was recorded in order to assess whether the oxidation of CO was complete. After several cycles between 0.05 and 1.1 V, the above potential-step experiment was repeated in the absence of adsorbed CO to record the current transients due to the

(11) Lucas, C. A.; Markovic, N. M.; Ross, P. N. *Surf. Sci.* **1999**, *425*, L381−L386.
(12) Markovic, N. M. The hydrogen electrode reaction and the electrooxidation of CO and H_2/CO mixtures on well-characterized Pt and Pt−bimetallic surfaces. In *Handbook of Fuel Cell Technology*; Vielstich, W., Lamm, A., Gasteiger, H., Eds.; John Wiley & Sons Ltd.: New York, 2002.
(13) Markovic, N. M.; Grgur, B. N.; Lucas, C. A.; Ross, P. N. *Surf. Sci.* **1997**, *384*, L805−L814.
(14) Friedrich, K. A.; Henglein, F.; Stimming, U.; Unkauf, W. *Electrochim. Acta* **2000**, *45*, 3283−3293.
(15) Friedrich, K. A.; Henglein, F.; Stimming, U.; Unkauf, W. *Electrochim. Acta* **2001**, *47*, 689−694.
(16) Cherstiouk, O. V.; Simonov, P. A.; Zaikovskii, V. I.; Savinova, E. R. *J. Electroanal. Chem.* **2003**, *554*, 241−251.
(17) Markovic, N. M.; Schmidt, T. J.; Grgur, B. N.; Gasteiger, H. A.; Behm, R. J.; Ross, P. N. *J. Phys. Chem. B* **1999**, *103*, 8568−8577.
(18) Sattler, M. L.; Ross, P. N. *Ultramicroscopy* **1986**, *20*, 21−28.
(19) Stamenkovic, V.; Chou, K. C.; Somorjai, G. A.; Ross, P. N., Jr.; Markovic, N. M. *J. Phys. Chem. B* **2005**, *109*, 678−680.
(20) Debe, M. K. Novel catalysts, catalysts support and catalysts coated membrane methods. In *Handbook of Fuel Cells: Fundamentals, Technology and Applications*; Vielstich, W., Lamm, A., Gasteiger, H., Eds.; John Wiley & Sons: New York, 2002; pp 576−589.
(21) Schmidt, T. J.; Gasteiger, H. A.; Stab, G. D.; Urban, P. M.; Kolb, D. M.; Behm, R. J. *J. Electrochem. Soc.* **1998**, *145*, 2354−2358.

pseudocapacitance of the electrode, that is, the so-called double layer charging curves. To assess the current transients that correspond exclusively to CO oxidation, the double layer charging curves were subtracted from the transients recorded in the first sets of experiments (see Supporting Information).

All electrochemical measurements were conducted in a standard three-compartment electrochemical cell. The reference electrode was a saturated calomel electrode (SCE) separated by an electrolytic bridge from the reference compartment. All potentials, however, are referenced to the potential of the reversible hydrogen electrode (RHE) calibrated from the hydrogen oxidation/reduction reaction measured in a rotating ring disk configuration in the same electrolyte. As counter electrode, a Pt mesh was used. The electrolyte was prepared using pyrolitically triply distilled water and concentrated $HClO_4$ (Aldrich, double distilled).

Infrared Spectroscopy. For measuring FTIR spectra on supported nanoparticles, we applied a new methodology, which has been recently described in detail in a separate paper.[22] In short, as for the electrochemical measurements, the catalyst was dispersed ultrasonically in water, and about 20 μL of the suspension was pipetted onto a heated (~130 °C) gold substrate (0.785 cm^2 geometrical surface area), cooled in an argon stream, and rinsed carefully with ultrapure water to remove loosely bound catalyst particles. No further attachment to the substrate was necessary. For the in situ FTIR measurements, a Nicolet Nexus 670 spectrometer was available equipped with a liquid N_2-cooled MCT detector. All IR measurements were performed in a spectroelectrochemical glass cell designed for an external reflection mode in a thin layer configuration.[23] The cell is coupled at its bottom with a CaF_2 prism beveled at 60° from the prism base. Prior to each experiment, the solution was saturated with argon. The electrode was immersed into the electrolyte at a potential of 0.05 V and a CV recorded. For the CO stripping measurements recorded in the spectroelectrochemical cell, the above-described two different adsorption procedures for obtaining a saturated CO adlayer, that is, oxide annealing and CO-annealing, were applied. Subsequently, all CO was removed from the solution by purging with argon for 20 min before pressing the sample onto the prism. Starting at 0.05 V, the potential was scanned with a scan rate of 1 mV/s in positive direction while continually recording spectra. To obtain a single spectrum, four interferometer scans were co-added. The recording time was thus reduced to ca. 2.5 s per spectrum. The resolution of the spectra was 4 cm^{-1}, and p-polarized light was used. Absorbance spectra were calculated as the ratio $-\log(R/R_0)$, where R and R_0 are the reflectance values corresponding to the sample and reference spectra, respectively. Reference spectra were recorded at either 0.95 V, where adsorbed CO (CO_{ad}) is completely oxidized, or at 0.05 V, well before the onset of CO_{ad} oxidation. The potential in the spectroelectrochemical cell was controlled by an SCE separated by a glass frit from the main compartment. All potentials, however, are referenced to the RHE calibrated from the hydrogen evolution/oxidation reaction in a separated cell using the same electrolyte.

3. Results and Discussion

3.1 Surface Characterization and Electrochemistry. Figure 1 shows representative low-magnification TEM images of Pt catalysts supported on carbon (Figure 1a−c) and on crystalline organic whiskers (Figure 1d). Although the nature of the support for the 30 nm particles is different, the catalytic properties of these particles are not affected by the nature of organic whiskers, as evidenced by comparing the catalytic activity of the oxygen reduction reaction on this catalyst and other bimetallic catalysts supported on whiskers to corresponding bulk electrodes. The

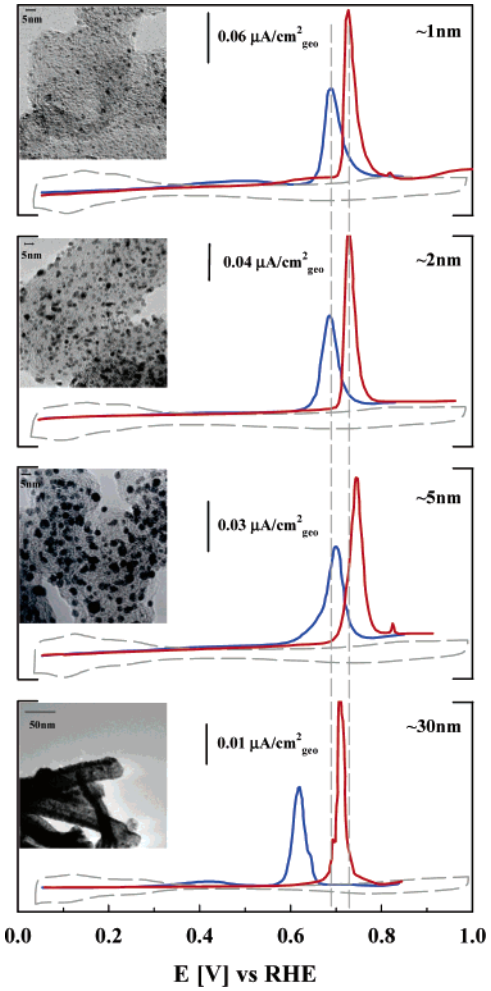

Figure 1. Comparison of CO stripping curves in 0.1 M $HClO_4$ solution purged after CO adsorption with argon for 30 min at 0.05 V; $T \sim 20$ °C, scan rate 1 mV/s; dashed gray curves show the respective base voltammogram (50 mV/s, currents multiplied by 1/50); the blue curves show the CO stripping curves after oxide-annealing (method I, see text) and the red curves after CO-annealing (method II, see text).

TEM images illustrate that the distribution of metal particles on the carbon support is rather uniform.

Histograms of the particle size distribution (not shown), which included analysis of several different regions of the catalysts, established that the average particle size of Pt supported on carbon is ca. 1, 2, and 5 nm. In agreement with Sattler and Ross,[9] lattice structure characterization obtained by high-resolution electron microscopy (HRTEM) revealed that although the basic shape of particles is cubooctahedral, the faces of the crystal are quite "rough" and "rounded" (i.e., as demonstrated in Figure 2b; the single crystal planes terminate in the surface in an irregular way, creating steps; furthermore, there are occasionally twinned particles which have an irregular surface). The presence of such "irregularities" on larger Pt particles (ca. ~30 nm) is even more obvious. The HRTEM image, depicted in Figure 2c, reveals the presence of defects, such as grain bounders and/or twins. From the TEM analysis, it appears that irregular surfaces of nanoparticles are the rule rather than the exception and, consequently, may play an important role in the observed particle size effect of the CO oxidation reaction.

Before we discuss the CO oxidation reaction, however, it would be appropriate to introduce the observed cyclic volt-

(22) Stamenkovic, V.; Arenz, M.; Ross, P. N.; Markovic, N. M. *J. Phys. Chem. B.* **2004**, *108*, 17915−17920.
(23) Iwasita, T.; Nart, F. C. *Prog. Surf. Sci.* **1997**, *55*, 271−340.

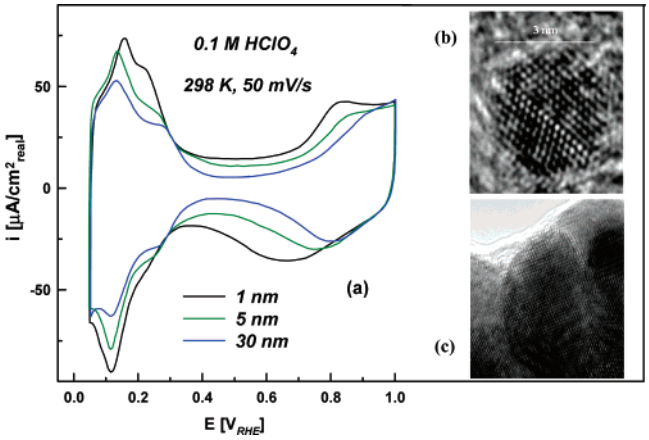

Figure 2. (a) Cyclic voltammograms of carbon-supported Pt catalyst samples recorded in 0.1 M $HClO_4$ solution; $T = 20$ °C, scan rate 50 mV/s; currents are normalized to the measured Pt surface area (H_{upd} charge after double layer correction); HRTEM images of a carbon-supported Pt nanoparticle (b), and the nanostructured Pt film supported on organic whiskers (c).

ammograms for the Pt nanoparticles attached to carbon and organic whiskers. The voltammograms for 1, 5, and 30 nm Pt catalysts (Figure 2) show three characteristic potential regions: the hydrogen adsorption potential region between 0.05 and 0.35 V is followed by the "double-layer" potential region, while above ~0.7 V, first OH adsorption and then oxide formation can be observed. Due to different loadings of the Pt catalysts as well as different contributions from the capacitance of the support, the comparison of CV's of high surface area catalysts is not as straightforward as established for extended single crystal surfaces.[3] Therefore, the cyclic voltammograms are "normalized" in terms of the specific surface area ($\mu A/cm_{Pt}^2$) obtained from the charge density for hydrogen adsorption/desorption corrected for the charging of the double layer. With this methodology, some trends in the adsorption/desorption properties of these catalysts can be established. For OH adsorption, the particle size dependence is less obvious; however, the oxophilicity of the catalysts appears to increase overall with increasing mean particle size. A small, yet clearly discernible, positive shift in the OH_{ad} formation is observed by a change in the particle size, that is, approximately 20 mV from 1 to 30 nm, while the onset for the 5 nm catalyst falls in between. This effect is more pronounced on the reversible sweep, where it is unambiguously shown that the peak for the oxide reduction shifts toward more negative potentials for the smaller particles, that is, about 130 mV for the 1 nm particles compared to the 30 nm particles. In agreement with oxide formation, the oxide reduction peak obtained for the 5 nm particles lies just between the one for the 1 and 30 nm particles, confirming previous findings that the oxophilicity of Pt particles increases by decreasing the particle size.[24−26] Assuming that CO oxidation on small particles obeys the Langmuir−Hinshelwood reaction mechanism

$$2H_2O \rightarrow OH_{ad} + H_3O^+ + e^- \quad (1)$$

$$CO_{ad} + OH_{ad} \rightarrow CO_2 + H^+ + e^- \quad (2)$$

which was previously proposed for extended surfaces;[3,27] the CO oxidation rate should increase in the same order as the oxophilicity of the Pt particles. In line with previous findings, however, Figure 1 unambiguously shows that the anodic CO stripping peak from 30 nm particles occurs at lower potentials compared to that of the particles with a size between 1 and 5 nm. A reason for this observation is still unclear, although Friedrich et al.[7,14,15] proposed that it originates from a stronger bonding of CO to the surface of smaller particles and a concomitant decrease in CO diffusion.

The puzzling particle size effect is further complicated by the observed difference in the CO stripping curves recorded on oxide-annealed and CO-annealed surfaces. Figure 1 shows that two different potential regions can be distinguished for both surfaces: (i) the so-called pre-ignition potential region ($0.05 < E < 0.55$ V), where only small currents are observed (especially on the electrode prepared by the CO-annealing method); and (ii) the potential region where sharp stripping peaks are observed in the cyclic voltammogram ($E > 0.55$ V). Further inspection of Figure 1 reveals that the CO stripping peak is shifted positively on the CO-annealed surfaces, consistent with the supposition that CO-annealed surfaces contain fewer irregularities than the respective surfaces that were never pretreated in CO-saturated solution. Finally, the CO stripping curves in Figure 1 indicate that, independent from the preparation method, the most active Pt catalyst (based on the position of the stripping peaks) is the one consisting of 30 nm particles. Interestingly, in contrast to the results in ref 10, the difference in the position of the stripping peaks for catalysts in the size range of 1−5 nm is subtle (at least for the sweep rate utilized in our experiments), that is, the most positive peak is the one obtained for the 5 nm particles, while those for the 1 and 2 nm particles are almost identical. Clearly, as for extended surfaces, for high surface area catalysts, it is very difficult to use the CO stripping peak as a measure for the particle size effect in CO oxidation. As we discuss below, to determine the onset potential for CO oxidation on the nanoparticle samples, we utilize the high sensitivity of IRAS to detect the O−C−O vibrational frequency of dissolved CO_2 as well as chronoamperometric measurements.

3.2 FTIR Measurements. In this section, the analysis and discussion of the FTIR results will be divided into two parts. First, we describe the vibrational properties of CO adsorbed on Pt nanoparticles pretreated by the oxide-annealing method, and then, we compare them to the results obtained for particles prepared by the CO-annealing method.

3.2.1 Pt Nanoparticles Pretreated by the Oxide-Annealing Method. In contrast to standard infrared spectral acquisition tactics where the potential is increased in steps of 50 or 100 mV, here, the spectra were recorded every 2.5 s during a positive potential sweep of 1 mV/s. A representative set of spectra obtained by the latter tactics on the 5 nm catalyst is summarized in Figure 3a (CO band) and b (CO_2 band).

The spectra in Figure 3a consist of a main band around 2060 cm^{-1}, which can be assigned to atop-bonded CO on Pt,[28] and a less pronounced CO band around 1880 cm^{-1}, which can

(24) Takasu, Y.; Ohashi, N.; Zhang, X.-G.; Murakami, Y.; Minagawa, H.; Sato, S.; Yahikozawa, K. *Electrochim. Acta* **1996**, *41*, 2595−2600.
(25) Mukerjee, S.; McBreen, J. *J. Electroanal. Chem.* **1998**, *448*, 163−171.
(26) Gasteiger, H. A.; Kocha, S. S.; Sompalli, B.; Wagner, F. T. *Appl. Catal., B* **2005**, *56*, 9−35.
(27) Markovic, N. M.; Grgur, B. N.; Lucas, C. A.; Ross, P. N. *J. Phys. Chem. B* **1999**, *103*, 487−495.
(28) Chang, S. C.; Weaver, M. J. *Surf. Sci.* **1990**, *238*, 142−162.

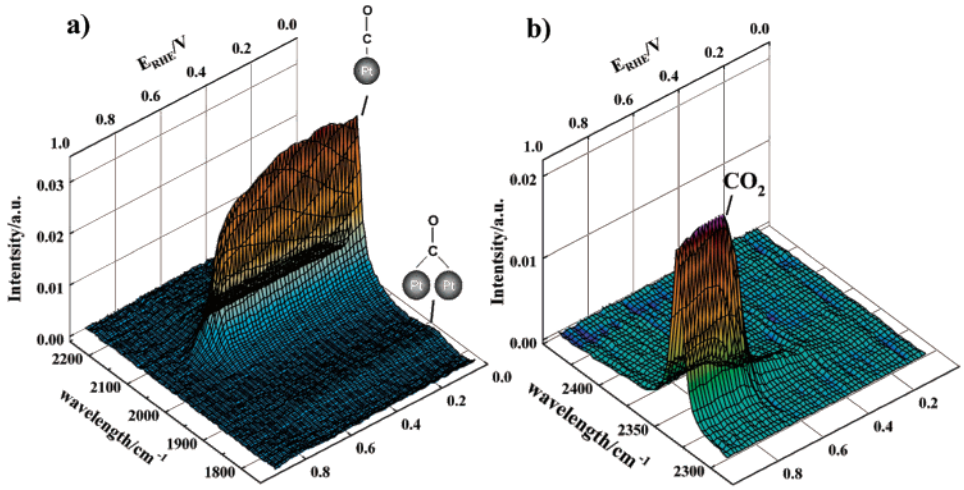

Figure 3. Representative CO stripping series of FTIR spectra (5 nm sample) recorded while scanning with 1 mV/s in argon-saturated $HClO_4$, every fifth spectra is depicted; (a) absorption band of atop and bridge-bonded CO; (b) CO_2 band.

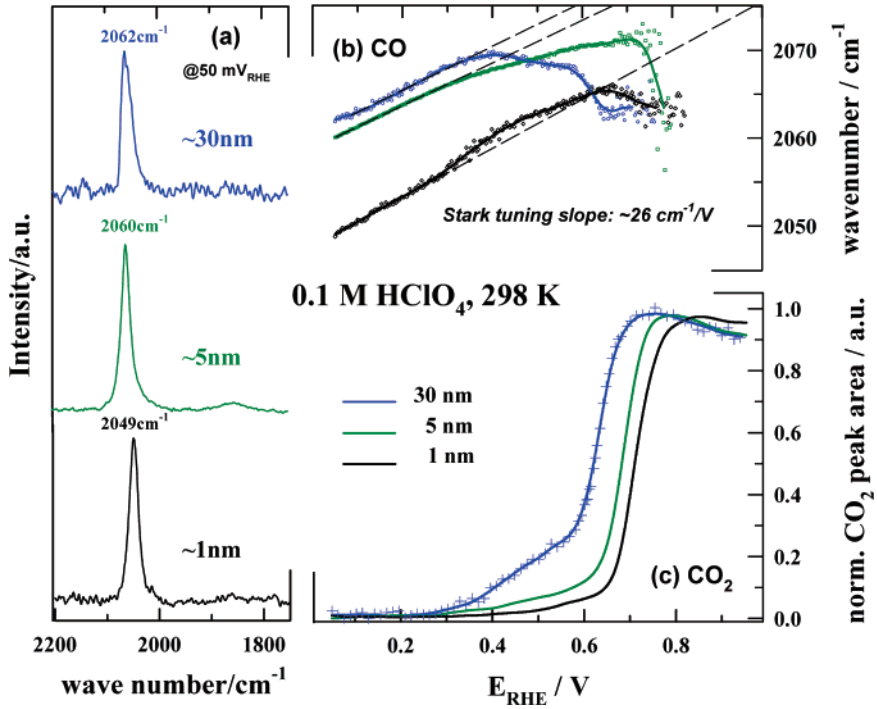

Figure 4. Summary of the results from the series of potential-dependent CO adsorption spectra for the different nanoparticle samples; measurements were taken in Ar-saturated solution after cycling in Ar-saturated solution and subsequent CO adsorption at 50 mV (method I); the potential was scanned with 1 mV/s while continuously recording spectra; the first spectra of the respective catalysts are given in part (a); the upper part (b) shows the potential dependent C−O stretch frequency of atop adsorbed CO; the lower part (c) compares the normalized peak area of CO_2 dissolved into solution (2343 cm^{-1}).

be assigned to bridge-bonded CO. The results obtained for the different catalyst samples are summarized in Figure 4 (for the sake of clarity, the results of the 2 nm sample are not shown here; see Figure 6). In agreement with previous measurements,[7,15,29] at 0.05 V, ν_{CO} redshifts as the particle size decreases, that is, from 2062 cm^{-1} on 30 nm particles to 2060, 2052, and 2049 cm^{-1} on 5, 2, and 1 nm particles, respectively.

The interpretation of the particle size-dependent C−O stretching frequency can be rationalized in terms of the chemical interaction between CO and Pt (chemical shift) as well as CO−CO lateral interactions (dipole−dipole coupling shift).[7,30,31] In particular, the decreased vibrational frequencies on small particles have been proposed to arise due to a stronger interaction of CO with the high density of edge−corner coordination in small nanoparticles, which is in line with detailed theoretical density functional (DFT) calculations[32,33] of CO chemisorbed on low-coordination sites, compared to terrace Pt sites, as well as a reduced dipole−dipole interaction of the CO adlayer.[34] It should be noted, however, that DFT calculations show no general link between the metal−CO binding energy

(29) Rice, C.; Tong, Y.; Oldfield, E.; Wieckowski, A.; Hahn, F.; Gloaguen, F.; Leger, J. M.; Lamy, C. *J. Phys. Chem. B* **2000**, *104*, 5803−5807.
(30) Severson, M. W.; Stuhlmann, C.; Villegas, I.; Weaver, M. J. *J. Chem. Phys.* **1995**, *103*, 9832−9843.
(31) Severson, M. W.; Weaver, M. J. *Langmuir* **1998**, *14*, 5603−5611.
(32) Hammer, B.; Norskov, J. K. In *Chemisorption and Reactivity on Supported Clusters and Thin Films*; Lambert, R. M., Pacchioni, G., Eds.; Kluwer Academic Publisher: Dordrecht, The Netherlands, 1997; p 285.
(33) Hammer, B.; Nielsen, O. H.; Norskov, J. K. *Catal. Lett.* **1997**, *46*, 31−35.
(34) Park, S.; Wasileski, S. A.; Weaver, M. J. *J. Phys. Chem. B* **2001**, *105*, 9719−9725.

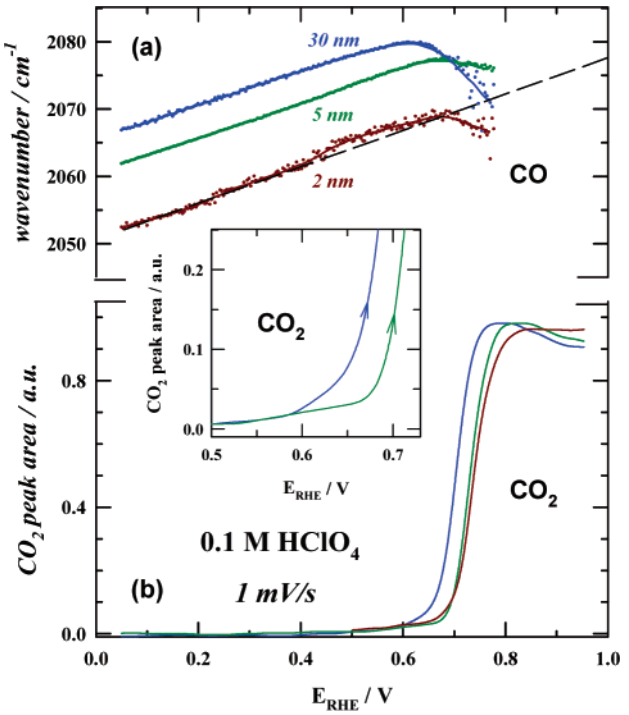

Figure 5. Summary of FTIR results of 2, 5, and 30 nm catalysts. In contrast to Figure 4, the CO adlayer was formed by the CO-annealing procedure (i.e., by cycling in CO-saturated solution for 5min, stopping at 0.05 V, and purging with Ar in order to remove all CO from solution (method II)).

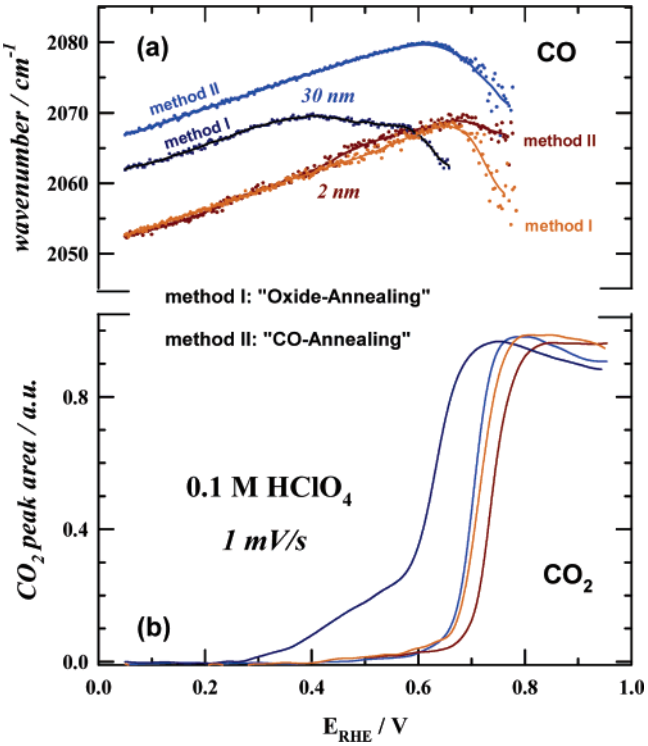

Figure 6. Comparison of CO adsorption/oxidation properties obtained with different CO adsorption procedures, CO-annealing and oxide-annealing (method I and II; for details, see text); blue colors: 30 nm sample; brown colors: 2 nm sample.

and the C−O stretching frequency.[35] On the basis of our measurements, we cannot state which effect is the predominant one and the correlation between the C−O vibrational frequency, and the detailed structure of the nanoparticles is far from being clear. To resolve this question, isotopic labeling measurements are suitable[36] and are currently performed on Pt single crystals using our FTIR methodology.

Figure 4a also shows that the CO bands are rather symmetrical with a bandwidth (fwhm) being almost independent of the particle size (ca. 20 cm^{-1}). This observation is at variance with previous findings, namely, that small particles exhibit a lower wavenumber "tail".[34,37] We recently suggested that the observed "tailing" is most likely an artifact that can completely be avoided by uniformly anchoring the metal nanoparticles onto the Au substrate.[22] Furthermore, Figure 4a shows that if the catalyst layer is uniformly dispersed on Au, then the fwhm is independent of the particle size.

The summary of the results from the series of potential-dependent CO adsorption spectra and the corresponding CO_2 production in Figure 4 serves to illustrate how the nanoparticle size affects the vibrational properties of CO_{ad} as well as the catalytic properties of Pt. As exemplified in Figure 4, for the 30 nm Pt particles, three potential regions can be discerned from the ν_{CO} versus E and the I_{CO_2} versus E plots. In the potential region ($0.05 < E < \sim 0.35$ V), where the CO adlayer is stable (no CO_2 production in Figure 4c), a linear frequency shift $d\nu/dE$ (25 cm^{-1}/V) is observed, consistent with the so-called electrochemical Stark-tuning effect.[38] Between ~0.35 and ~0.60 V, however, the Stark-tuning slope, $d\nu/dE$, changes its sign, while simultaneously, a weak CO_2 band is detected in the spectra, indicating a slow but finite CO oxidation rate. In line with our previous discussion of the Pt(*hkl*)−CO system,[3] the potential range where the CO oxidation rate is rather small, we define as the pre-ignition potential region. Finally at $E \sim 0.60$ V, the so-called ignition potential, we observe a fast increase in I_{CO_2} as well as a substantial change in $d\nu/dE$, directly indicative of facile CO oxidation.

The spectral data of the 5 nm particles in Figure 4b reveal some important differences as well as some similarities with the 30 nm particles. As for larger particles, a linear positive Stark-tuning slope of ~25 cm^{-1}/V is observed over the potential region where no CO_2 is detected, $0.05 < E < \sim 0.35$ V. At $E > 0.35$ V, the slope starts to decrease, but in contrast to the 30 nm particles, it still remains positive all the way up to 0.7 V. The small change in the Stark-tuning slope is accompanied by the appearance of a relatively weak CO_2 band. Although the onset potential for CO_2 production is the same on the 5 and 30 nm particles, Figure 4c shows that at low potentials, the integrated intensities for the CO_2 band are much lower for the 5 nm particles, suggesting that the rate of CO_2 production is much smaller on the 5 nm particles than on the 30 nm particles. The confirmation that the oxidative removal of CO_{ad} on 30 nm particles is faster than that on 5 nm particles is also obtained from the ignition potential region (the negative $d\nu/dE$ slope and extensive production of CO_2), which is on the 5 nm catalyst shifted by ca. 50 mV toward higher potentials.

For very small Pt nanoparticles (1 and 2 nm), we observe an anomalous behavior in the $\nu_{CO}-E$ frequency shift, which to our knowledge for the case of nanoparticles, has not yet been

(35) Shubina, T. E.; Koper, M. T. M. *Electrochim. Acta* **2002**, *47*, 3621−3628.

(36) Chang, S. C.; Roth, J. D.; Weaver, M. J. *Surf. Sci.* **1991**, *244*, 113−124.
(37) Park, S.; Tong, Y.; Wieckowski, A.; Weaver, M. J. *Electrochem. Commun.* **2001**, *3*, 509−513.
(38) Bishop, D. M. *J. Chem. Phys.* **1993**, *98*, 3179−3184.

reported in the literature. For 1 nm particles, this anomalous behavior is more pronounced than that for 2 nm particles, and in the following, we will focus on the CO vibrational/catalytic properties on 1 nm particles. Figure 4b shows that around 0.35 V, the Stark-tuning slope first slightly increases then while still remaining positive, at $E > 0.55$ V, begins to decrease, and finally at 0.7 V, where the rapid CO oxidation occurs, a negative sign in $d\nu/dE$ is observed. Interestingly, the blueshift deviations in the ν_{CO} frequency are accompanied by a small yet clearly discernible CO_2 production, indicating that although the surface is less covered by CO, the interaction energy of CO with the Pt particles is weaker! Note that we were able to observe a similar blueshift in the ν_{CO} frequency at the onset of CO oxidation on Pt(111).[19] For the Pt(111)−CO system, we suggested that the initial CO oxidation is accompanied by adsorption of anions from the supporting electrolyte. We also argued that co-adsorbed anions may lead to a compression of CO molecules, resulting in a higher local CO coverage thus yielding blueshifted atop CO frequencies due to enhanced dipole−dipole coupling. Notice that the phenomenon of island compression is observed in segregated systems where the presence of one species causes the other species to segregate into patches in which the local density is higher than that observed when an equivalent amount of particular species is adsorbed alone (see for example ref 39). Extending this phenomenon to CO adsorbed on Pt nanoparticles, the surprising blueshift in the ν_{CO} frequency for 1 nm particles at $E > 0.3$ V may be a consequence of slow but continuous CO oxidation which is accompanied by anion adsorption (either ClO_4^- [40] or trace levels of Cl^- impurities[41]) and concomitant CO compression on (111) facets. Furthermore, the close similarity between the vibrational properties of CO adsorbed on Pt single crystals and very small Pt nanoparticles is in line with the TEM analysis, which showed that the surface of large particles contains undistorted (111) facets in a smaller fraction in contrast to the surface of small particles.

To conclude this section, we have shown that while the onset potential for CO oxidation is almost independent of the particle size, the rate of CO_2 production strongly depends on the particle size, that is, $1 \leq 2 < 5 \ll 30$ nm. Closely following the interpretation of the CO oxidation rate in the pre-ignition region on extended Pt single crystal surfaces, in the next section, we suggest that I_{CO_2} is controlled by the presence of specific surface irregularities (see section 3.1), which serve as nucleation center for OH adsorption.

3.2.2 Pt Nanoparticles Pretreated by the CO-Annealing Method. For the purpose of our discussion here, we present the ν_{CO} versus E plots for the 30, 5, and 2 nm particles.

As shown in Figure 5a and in agreement with the results shown in Figure 4, by decreasing the particle size, the CO band position shifts toward lower wavenumbers, that is, from 2067 to 2062 and 2052 cm^{-1} for 30, 5, and 2 nm particles, respectively. As discussed in refs 7 and 15 and section 3.2.1, the observed redshift can be rationalized by an interplay between the chemical shift (stronger CO adsorption on smaller nanoparticles) and the dipole shift (enhanced CO−CO lateral interactions on larger particles). Further inspection of Figure 5a shows that for 30 nm particles, the "normal" Stark-tuning behavior, with a slope of ~25 cm^{-1}/V, is observed from 0.05 to 0.65 V, that is, just prior to the occurrence of significant CO oxidation, monitored by an extensive CO_2 production (Figure 5b). For 5 nm particles, a linear Stark-tuning slope of ~25 cm^{-1}/V is also clearly observed between 0.05 and 0.7 V. On both catalysts, a small CO_2 production is observed at potentials as low as 0.6 V (see the insert of Figure 5). Intriguingly, on 2 nm particles, the anomalous blueshift deviation from the normal Stark-tuning slope is observed over the potential range of $0.55 < E < 0.7$ V. Again, the observed deviation coincides with a small yet clearly discernible CO_2 production (Figure 5b), confirming that the blueshift deviation is triggered by the slow oxidation of CO. If we use I_{CO_2} as a measure for the catalytic activity, then the CO oxidation rate increases in the order 30 > 5 > 2 nm.

3.2.3 Effect of Surface Irregularities. In Figure 6, we compare the IRAS data for the two different pretreatments of the nanoparticle catalysts. For the 30 nm particles, ν_{CO} on the CO-annealed surface is blueshifted by ca. 5 cm^{-1} relative to the surface pretreated by the oxide-annealing method. If correlated to the CO bonding energy, the observed blueshift would imply that the Pt−CO interaction is weaker with the CO-annealed than with the oxide-annealed nanoparticles. The CO_2 production in Figure 6b, however, is higher on the latter surface, showing that the C−O stretch of Pt-bound CO is no indication for the catalytic activity of the CO adlayer.

Since we observed that surfaces containing more irregularities, such as the oxide-annealed 30 nm particles, are more reactive, we suggest that the oxidation rate of a CO monolayer (CO stripping conditions) is controlled by the presence of catalytically active OH which is formed on defect sites rather than by the Pt−CO energetics, that is, the CO mobility. This is in agreement with our findings that on Pt single crystal surfaces, the CO oxidation rate is more influenced by the ability of the surface to dissociate water and to form OH_{ad} on defect sites than by CO energetics.[17,42,43] Defect sites also play a role in CO "clustering" on the 30 nm nanoparticles, causing CO to decrease in local coverage on the oxide-annealed surface relative to the CO-annealed surface. Consequently, the higher local CO coverage on the latter surface yields to blueshifted ν_{CO} frequencies due to enhanced dipole−dipole coupling, as shown in Figure 6a.

In this context, it is also worth mentioning that over the potential range of $0.05 < E < 0.5$ V, the ν_{CO} frequency on the 2 nm particles (as well as on the 1 nm particles) is independent from the preparation procedure. This observation is consistent with the TEM analysis showing that the "surface roughness" of the cubooctahedrons increases with the particle size and, thus, the vibrational properties of CO_{ad} on smaller particles are less affected by the preparation method. The importance of defects is, however, observed at potentials $E > 0.5$ V, where a small production of CO_2 on CO-annealed particles is accompanied by an increase in the C−O vibrational frequency. Notice that the blueshift deviations from the normal Stark-tuning slope are more pronounced on the CO-annealed, that is, the less irregular

(39) McIntyre, B. J.; Salmeron, M.; Somorjai, G. A. *Surf. Sci.* **1995**, *323*, 189−197.
(40) Ataka, K.; Yotsuyanagi, T.; Osawa, M. *J. Phys. Chem.* **1996**, *100*, 10664−10672.
(41) Arenz, M.; Stamenkovic, V.; Schmidt, T. J.; Wandelt, K.; Ross, P. N.; Markovic, N. M. *Surf. Sci.* **2003**, *523*, 199−209.
(42) Grgur, B. N.; Markovic, N. M.; Ross, P. N. *J. Phys. Chem. B* **1998**, *102*, 2494−2501.
(43) Markovic, N. M.; Lucas, C. A.; Grgur, B. N.; Ross, P. N. *J. Phys. Chem. B* **1999**, *103*, 9616−9623.

2 nm particles. Most likely, the microscopic effect responsible for the observed differences in the ν_{CO} frequency is the same as the one proposed for the 30 nm particles; that is, the smaller number of defects on the CO-annealed surface allows CO to increase in local coverage accounting for the observed blueshift in the ν_{CO} frequencies due to enhanced dipole−dipole coupling. As for the 30 nm nanoparticles, the "high-frequency CO" on the 2 nm nanoparticles is less reactive than the "low-frequency CO", which intuitively can be explained more easily by the availability of defect sites for OH adsorption than by Pt−CO energetics. Therefore, considering that surfaces of larger particles are inherently rougher than those of smaller particles, the order of reactivity for CO monolayer oxidation (CO stripping) increases by increasing the size of the Pt nanoparticles. Along the same lines, because CO-annealed surfaces contain fewer defects than oxide-annealed surfaces, oxidative removal of CO on particles with nominally the same size is enhanced on the oxide-annealed surface.

3.3 Chronoamperometric Measurements. Additional information about the particle size effect on the oxidative removal of CO is obtained from chronoamperometry experiments. The same method has been used previously by Love et al.[44] as well as by Lebedeva et al.[45] for studying the role of crystalline "defects" on the rate of CO oxidation on Pt(*hkl*) and stepped Pt single crystal surfaces, respectively. The authors found that an increase in the step density for Pt(*hkl*) from the [1$\bar{1}$0] zone results in a systematic negative shift of the CO stripping peak, consistent with the previous suggestion[17] that low-coordination sites may serve as active centers for OH adsorption and, thus, oxidative removal of CO. The current−time transients for the oxidation of a CO-saturated adlayer have been successfully modeled by using the mean-field approximation of the L−H mechanism, which implies fast diffusion of CO adsorbed on the terraces of the Pt stepped single crystal surfaces. By contrast, Maillard et al. suggested that for *ideal* cubooctahedral Pt nanoparticles, the stepped single crystal surfaces could not be used as an adequate model for understanding the shape of the CO oxidation current transients.[10] The model for the *perfect* cubooctahedral particle suggested restricted CO mobility at Pt nanoparticles below ca. 2 nm size and a transition toward fast diffusion when the particle size exceeds 3 nm. Unfortunately, the model did include neither the competitive adsorption of bisulfate anions (which can control the adsorption of OH as well as the mobility of co-adsorbed CO[19]) nor the existence of irregularities on nanoparticles that, as for the extended single crystal surfaces, may serve as the active centers for OH adsorption. In the following, we use the chronoamperometric method to get further insight into the effect of surface irregularities on the reactivity of Pt nanoparticles in CO monolayer oxidation.

3.3.1 Potentiostatic Conditions. Figure 7 shows the transient currents for CO oxidation on 1 nm Pt particles as the potential is stepped from 0.05 V to five more positive potentials that are designated on a corresponding cyclic voltammogram (see insert). Curves 1 and 2 represent the current transients for CO oxidation in the preoxidation region; curve 3 shows a potential step at

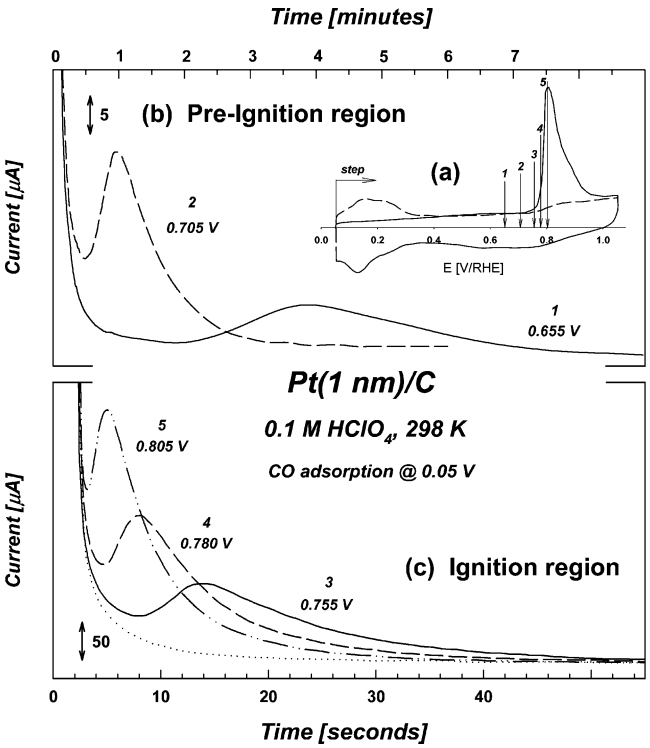

Figure 7. Chronoamperometric measurements of CO adlayer oxidation on 1 nm particles in 0.1 M HClO4; CO was adsorbed at 50 mV, and the final potential was chosen in the pre-ignition (a) as well as in the ignition potential region (b); the insert indicates the respective potentials in the corresponding CO stripping voltammetry.

the ignition potential, and curves 4 and 5 are characteristic representatives for the transients observed within the ignition potential region. These examples characterize the general pattern of induction periods, that is, the time required for a system to pass from an inactive state (charging of the double layer) to active state (the onset of CO oxidation), as well as the shape of current transients. As expected, the induction time is longer (by orders of magnitude) in the preoxidation region (Figure 7a) than at or above the ignition potentials (Figure 7b), consistent with the proposition that the rate of oxidative removal of CO in stripping experiments depends on the number of sites on which OH can be adsorbed. The same argument can be used to rationalize the observation that the time required to reach the maximum current, as well as to completely oxidize CO, is shorter after stepping to more positive potentials.

Even though the same potential-step experiments were conducted for 2, 5, and 30 nm Pt nanoparticles, only selected results for CO monolayer oxidation on 2 and 30 nm particles will be presented and compared with the results for the 1 nm particles. Figure 8 summarizes representative transients for CO oxidation on the three different nanoparticles, along with the charging curve of the "double layer" (dotted curves), that is, after stepping from 0.05 V to the same final potentials but on CO-free surfaces. Figure 8 a′−c′ shows the difference between the transient for CO oxidation and the charging of the double layer, that is, the true transients for CO oxidation. Clearly, the particle size generates quite significant changes in the CO transient curves. (i) The induction period decreases by increasing the particle size, consistent with the FTIR results that larger particles are more active for CO oxidation. (ii) While on the 1 nm particles a well-defined single maximum (characteristic for

(44) Love, B.; Lipkowski, J. Effect of surface crystallography on electrocatalytic oxidation of carbon monoxide on Pt electrodes. In *Molecular Phenomena at Electrode Surfaces*; Soriaga, M. P., Ed.; American Chemical Society: Washington, DC, 1988; pp 484−496.
(45) Lebedeva, N. P.; Koper, M. T. M.; Feliu, J. M.; van Santen, R. A. *J. Phys. Chem. B* **2002**, *106*, 12938−12947.

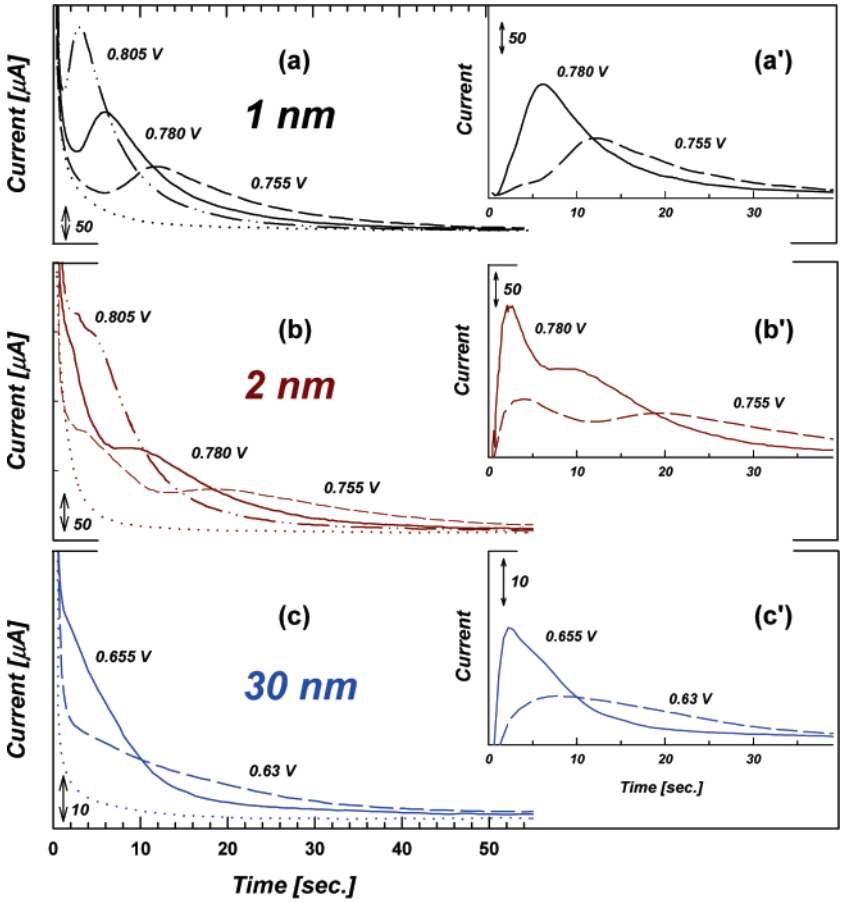

Figure 8. Chronoamperometric measurements of (a) 1, (b) 2, and (c) 30 nm particles, as recorded current−time transients (left-hand side), transients after correction of the double charging/discharging transients (the right-hand side); initial potential of 0.05 V, final potential as indicated.

current transients on Pt single crystals[46]) is observed, on the 2 nm particles, current transients can be deconvoluted into two peaks, one that appears within 5 s and the other that is developed after 10 s (0.780V), suggesting that 1 nm particles are more "ideal" cubooctahedrons than are the 2 nm particles. (iii) The oxidation of CO on 30 nm particles is so fast that no apparent current maximum is observed in the current transients. Note that because the CO oxidation on the 30 nm particles is much faster than on the other three, the final positive potential on the former catalyst is at 0.63 and 0.655 V.

In Figure 9, we compare the chronoamperometric data for CO oxidation on the 1 nm catalyst pretreated either by the oxide-annealing procedure (red curves) or by the CO-annealed procedure (blue curves). In these experiments, by changing the number of irregularities while keeping the same size of the particles, the intention is to study the effect of the density of active sites for OH adsorption on the induction period and current relaxation during CO oxidation. As expected, the induction period increases by decreasing the number of irregularities on the CO-annealed surface. In addition, the time required to reach the current maximum is shorter for the oxide-annealed than for the CO-annealed surfaces, in agreement with our discussion above that the initial oxidation rate depends on the number of active sites for OH adsorption (in the Supporting Information, we also show the results for 2 nm).

On the basis of these observations, and in light of our discussion in the previous section, it becomes obvious that the puzzling size effects on the reactivity of Pt nanoparticles in CO monolayer oxidation (CO stripping) can be explained by considering how the fraction of irregularities (defects), surface atoms in (111), (100) facets, and edge−corner sites may effect the rate of the oxidative removal of CO from a real nanoparticle. In our previous report for CO oxidation on Pt(111),[17] we argued that on the surface, which is *completely* covered by CO, the initial adsorption of OH (i.e., the initial CO oxidation) takes place at *defects* in the (111) surface. This is confirmed from the results published later for the CO stripping on the Pt stepped single crystal surfaces.[45−47] We also suggested that in acid solutions there is a strong competition for the active sites between the OH and anions from the supporting electrolyte. Initially, on the surface fully covered by CO, the adsorption of relatively small OH ions will be predominant because of geometric considerations, even though at low overpotentials ($0.05 < E < 0.7$ V), specific adsorption of relatively large anions would be thermodynamically more favorable. As the CO oxidation proceeds, however, the anion adsorption will be possible on CO-free Pt sites. Consequently, anions can block the further adsorption of OH that, in turn, will affect the rate of CO oxidation and the observed tailing. In addition to the blocking effect, the adsorbed anions may also affect the diffusion

(46) Lebedeva, N. P.; Koper, M. T. M.; Feliu, J. M.; van Santen, R. A. *J. Electroanal. Chem.* **2002**, *524*, 242−251.

(47) Lebedeva, N. P.; Koper, M. T. M.; Herrero, E.; Feliu, J. M.; van Santen, R. A. *J. Electroanal. Chem.* **2000**, *487*, 37−44.

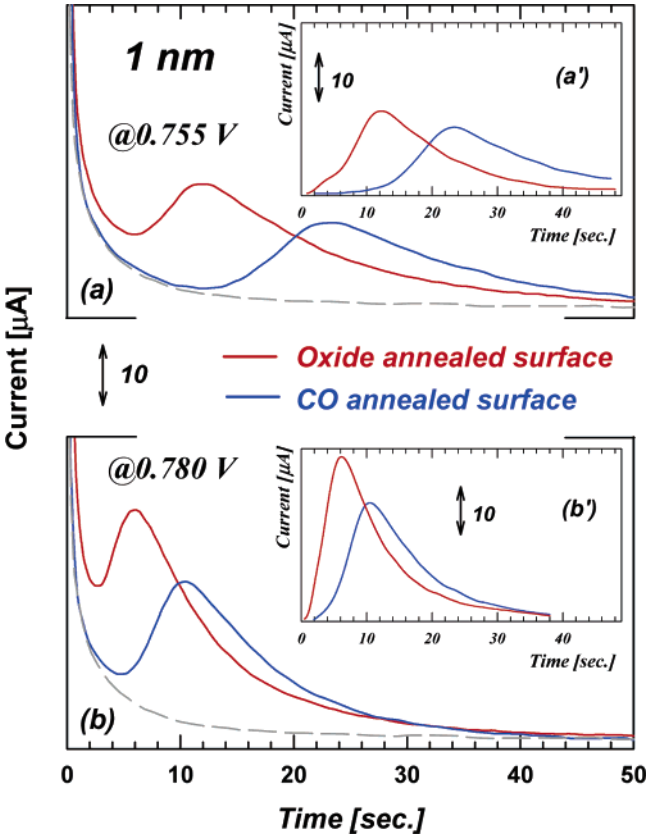

Figure 9. Comparison of chronoamperometric measurements on the oxide and CO-annealed surface of the 1 nm sample; insert: double layer corrected current−time transients; initial potential of 0.05 V, final potentials as indicated.

as well as the clustering of CO, as we discussed in the FTIR section. Closely following this discussion, it is plausible that the observed tailing observed at Pt nanoparticles below 2 nm[10] is affected rather by the influence of anions on CO diffusion than by the energetics of the Pt−CO interaction. To conclude, in the future, the modeling of CO oxidation current transients would require the specific adsorption of anions to be taken into consideration, as well.

3.4. RDE Measurements of CO Bulk Oxidation. Although CO stripping curves and chronoamperometric measurements provide valuable information on the oxidative removal of CO, in fuel cell applications, the anode catalyst experiences a continuous supply of CO to the surface, which can be simulated in RDE measurements. We found for CO bulk measurements, that is, RDE measurements in CO-saturated solution, that if the surface is completely covered by CO, the difference in catalytic activity between the four Pt catalysts is negligible in the positive going sweep. Interestingly, in gas-phase catalysis, McCarthy et al.[48] found that under high CO partial pressure conditions (equivalent to our experimental conditions when surface is completely covered by CO), the specific rate is "facile" (insensitive to the particle size) but "demanding" (structure sensitive[49]) for low CO partial pressure. Under the latter conditions, the specific rate is higher for low area (sintered) Pt. It has been suggested that the observed deactivation with decreasing particle size stems most likely from the build-up of

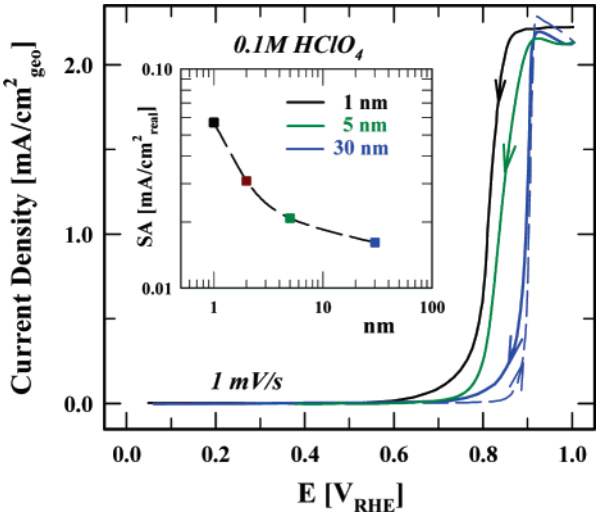

Figure 10. Rotating disk electrode measurements of CO bulk oxidation on 1, 5, and 30 nm catalysts in 0.1 M $HClO_4$ solution constantly purged with CO; CO adsorption at 0.05 V, $T \sim 20$ °C, scan rate 1 mV/s, rotation rate 1600 rpm; positive sweep shown only for 30 nm (others are identical), positive limit 1.0 V; insert: logarithmic plot of specific activity for CO_b−ox at 0.8V obtained at cathodic sweep versus particle size.

a nonreactive oxygen species,[50] in a manner similar to that observed by Ostermaier et al.[51] for ammonia oxidation over Pt. In electrocatalysis, it has also been found that under different experimental conditions, either a nonreactive oxide ($E >$ 1.1 V) or a reactive oxide (termed as OH_{ad}; $E <$ 1.1 V) can build up on the surface. To test how the build-up of *reactive* oxygen affects CO oxidation on Pt nanoparticles in an electrochemical environment, polarization curves were recorded upon sweep reversal at 1.0 V, where the surface is predominantly covered by reactive oxygenated species. The results in Figure 10 clearly show that if the electrode is predominately covered by oxide, the CO oxidation reaction is demanding and the activity of Pt nanoparticles increases in opposite order to that observed in CO stripping experiments (30 < 5 < 2 < 1 nm). Clearly, in the case of the CO oxidation reaction, depending upon the reaction conditions, small particles are able to exhibit higher or lower specific activity than larger ones. For example, because the isosteric heat of CO adsorption on Pt(*hkl*) is relatively insensitive to the surface structure, it is reasonable to suggest that if the surface is completely covered by CO (high-pressure conditions), the Pt−CO energetics will play a negligible role in the kinetics of CO oxidation.

By contrast, the number of defects on which the initial adsorption of reactive OH will occur is very important, so that the rate of oxidative CO removal in CO stripping experiments increases with the availability of those sites, that is, 1 < 2 < 5 < 30 nm. However, under experimental conditions in which the surface is predominantly covered by OH_{ad} (oxide), the reversed order in activity is obtained, consistent with the fact that the heat of oxide formation increases by increasing the number of low-coordinated surface atoms (see voltammetry in Figure 2). Given that at the adsorbate-free nanoparticle the fraction of active edge−corner sites is larger than the defect sites and considering that the surface distribution of the former

(48) McCarthy, E.; Zahradnik, J.; Kuczynski, G. C.; Carberry, J. J. *J. Catal.* **1975**, *39*, 29−35.
(49) Boudart, M. *Adv. Catal.* **1969**, *20*, 153.
(50) Cant, N. W. *J. Catal.* **1980**, *62*, 173−175.
(51) Ostermaier, J. J.; Katzer, J. R.; Manogue, W. H. *J. Catal.* **1974**, *33*, 457−473.

sites increases by decreasing the particle size,[52] then small particles are more oxophilic. Thus, at high overpotentials, they provide more active sites for the oxidative removal of adsorbed CO. Therefore, depending on the experimental conditions, the ratio between the availability of "defects" versus "ideal" sites is changing, from highly available defect sites on an electrode fully covered by CO, which is determining the induction period and the shape of current transients in the CO stripping experiments, to a high fraction of available regular facets and edge−corner sites at the surface predominately covered by oxide, which determines the rate of CO bulk oxidation.

4. Conclusion

Platinum particles ranging in size from 1 to 30 nm were characterized and evaluated for their catalytic activity for CO electrooxidation, using high-resolution transmission electron microscopy, infrared reflection−absorption spectroscopy, and electrochemical measurements. The results can be summarized as follows:

(1) TEM analysis shows that the Pt crystallites are, in general, *not* perfect cubooctahedrons, and that the particles provide a variety of low-coordination sites for adsorption and catalysis. We found that large particles are quite "rough", containing irregular steps and occasionally twinned particles. On the other hand, the smallest particles show mostly regular facets and uniform edge−corner sites as expected from perfect cubo-octahedrons.

(2) The surface sensitivity for the oxidative removal of adsorbed CO was probed in IRAS experiments by monitoring the potential dependence of the atop CO vibrational frequency and the concomitant development of asymmetric O−C−O stretch of dissolved CO_2. It was found that while the onset potential of CO oxidation is almost independent of the particle size, the rate of CO_2 production is strongly dependent on the particle size (i.e., $1 \leq 2 < 5 \ll 30$ nm). We suggest that the oxidative removal of CO is mainly controlled by the number of defects, which in an ideal cubooctahedral particle may serve as an active center for OH adsorption. It was also found that, depending on the particle size (d), the onset of CO_2 production is accompanied either by redshift ($d > 5$ nm) or by anomalous blueshift ($d < 2$ nm) deviations from the normal Stark-tuning slope. The interpretation of the anomalous $d\nu_{CO}/dE$ behavior is discussed in relation to similar changes observed at the Pt(111)−solution interface, that is, in terms of slow CO oxidation, co-adsorption of anions, and concomitant CO compression into small islands on fairly smooth (111) facets.

(3) Chronoamperometric measurements indicate that the observed tailing in the transients on small Pt nanoparticles is rather due to the influence of co-adsorbed anions on CO surface diffusion than by the energetics of the Pt−CO interaction. In the future, the modeling of CO oxidation current transients would require the specific adsorption of anions and irregular particle shapes to be taken into consideration, as well.

(4) In contrast to CO adlayer stripping, we found that the oxidation kinetics of dissolved CO on an OH_{ad}-covered surface increase by decreasing the particle size, that is, more oxophilic small particles are more active for bulk CO oxidation than are larger particles. Therefore, the observed particle size effect strongly depends on the experimental conditions.

Acknowledgment. This work was supported by the Director, Office of Science, Office of Basic Energy Sciences, Division of Materials Sciences, U.S. Department of Energy under Contract No. DE-AC03-76SF00098. We thank Dr. V. Radmilovic from the National Center for Electron Microscopy for his expertise in analyzing the TEM images, as well as Dr. R. Atanasoski and Dr. M.K. Debe from the 3M Corporation for supplying one of the catalyst samples. K.M. acknowledges the Austrian BMBWK for a Ph.D. scholarship. M.A. is grateful for a Feodor Lynen fellowship from the German Alexander von Humboldt foundation.

Supporting Information Available: Figures showing the current−time transients and a comparison of the chronoamperometric measurements of the oxide CO-annealed surface of the 2 nm sample. This material is available free of charge via the Internet at http://pubs.acs.org.

JA043602H

(52) Kinoshita, K. *Electrochemical Oxygen Technology*; John Wiley & Sons: New York, 1992.